Designing bioinspired parahydrophobic surfaces by electrodeposition of poly(3,4-ethylenedioxypyrrole) and poly(3,4propylenedioxypyrrole) with mixed hydrocarbon and fluorocarbon chains

Elhadji Yade Thiam, Abdoulaye Drame, Aboubacary Sene, Samba Yandé Dieng, Frédéric Guittard, Thierry Darmanin

Designing bioinspired parahydrophobic surfaces by electrodeposition of poly(3,4-ethylenedioxypyrrole) and poly(3,4-propylenedioxypyrrole) with mixed hydrocarbon and fluorocarbon chains

Elhadji Yade Thiam[a], Abdoulaye Drame[a], Aboubacary Sene,[a] Samba Yandé Dieng[a], Frédéric Guittard[b,c], Thierry Darmanin[b]*

[a]*Université Cheikh Anta Diop, Faculté des Sciences et Techniques, Département de Chimie, B.P. 5005 Dakar, Sénégal*

[b]*Université Côte d'Azur, NICE Lab, IMREDD, 61-63 Av. Simon Veil, 06200 Nice, France*

Fax: (+33)492076156; Tel: (+33)492076159;

E-mail: thierry.darmanin@unice.fr

[c]*University California Riverside, Department of Bioengineering, Riverside, CA, USA*

Abstract

In the aim to tune the surface nanostructures and the resulting surface hydrophobicity and water adhesion, we report the preparation of surfaces by electropolymerization of 3,4-ethylenedioxypyrrole (EDOP) and 3,4-propylenedioxypyrrole (ProDOP) with both a short fluorocarbon chain (C_4F_9) and an alkyl chain of various length (C_2H_5 to $C_{12}H_{25}$). The surface properties are very different following the choice of the polymerizable core (EDOP or ProDOP) and the alkyl chain length. The PEDOP polymers are here easier to electrodeposit while the ProDOP could be electrodeposited only with long alkyl chains ($\geq C_8H_{17}$). Their electrodeposition leads to the formation of both nanoparticles and wrinkles. The highest properties with apparent contact angle (θ_w) $\approx$ 141° and extremely strong water adhesion (parahydrophobic properties) are obtained with EDOP monomers and using intermediate alkyl chains (C_6H_{13} and C_8H_{17}). Such properties could be exploited in the future in

applications where the control of the interaction forces with the media is required such as in oil/water separation membranes or in water harvesting systems.

Keywords: Hydrophobicity, Adhesion, Nanostructures, Electropolymerization, Conducting Polymers.

1. Introduction

Controlling the surface wettability is fundamental for various practical applications for example in waterproof textiles, oil/water separation membranes, microfluidic devices, non-stick pans, water harvesting systems, anti-icing windows or antifouling paints [1-4]. The bioinspiration and biomimicry allowed to solve complex wettability problems [5-7]. Indeed, they are numerous species in Nature with special wettability properties. This is case of the superhydrophobicity, characterized by high water apparent contact angle and low water adhesion [8-10]. This property is presence in various species allowing to have strategic advantages such as self-cleaning, anti-fogging properties, or the capacity to slide on the water surface. Other species such as rose petals have the capacity to trap water droplets even in arid or hot environments thanks to surfaces with parahydrophobic surfaces characterized by high water apparent contact angle but high water adhesion [11-14]. All these examples have allowed to find to key parameters for the control of surface wettability, which are the surface energy and the surface roughness/structuration.

The strategies to control both the surface structures and the surface energy are numerous in the literature and are generally classed in two categories called top-down and bottom-up approached [15-19]. To prepare structured surfaces, the electropolymerization, one of the bottom-up approaches, is a very interesting and fast technique with a control by electrochemical parameters and the monomer structure [20-24]. This technique consists in the electrochemical oxidation of a monomer to deposit conducting polymer films on a working electrode. In order to control also the surface energy, substituents can be easily grafted on the monomer. For example, linear hydrocarbon or fluorocarbon chains are often used for

superhydrophobic properties while branched hydrocarbon chains or aromatic groups for parahydrophobic properties.

The monomers of the 3,4-alkylenedioxypyrrole (XDOP) family such as 3,4-ethylenedioxypyrrole (EDOP) and 3,4-propylenedioxypyrrole (ProDOP) have ultra-low exceptional potential and lead to polymers with unique opto-electronic properties including high conductivity, multicolor cathodic and anodic electrochromism, and rapid redox switching [25-28]. Moreover, substituents can be grafted not only on the nitrogen [29] but also on the 3,4-alkylenedioxy-bridge [30,31]. However, the substitution often needs multiple chemical reaction for each monomer. Very recently, thanks to a reaction with epibromohydrin, we found a strategy to prepare both EDOP and ProDOP platform molecules with hydroxyl group, easy to functionalize [32]. For example, fibrous structures with exceptional anti-wetting properties were obtained but only with short fluorocarbon chains (C_4F_9), compared to longer fluorocarbon chains (C_6F_{13} and C_8F_{17}). Moreover, short fluorinated chains such as C_4F_9 chains are expected to have less bioaccumulative potentials compared to long fluorinated chains and potentially less persistent in the environment [33-35]. To go further in this direction, here, we wanted to investigate the influence of mixed hydrocarbon and fluorocarbon chains on both the surface morphology and wettability. As shown in Scheme 1, we kept a short C_4F_9 from the previous results [32] and changed the length of the hydrocarbon chain from C_2 to C_{12}.

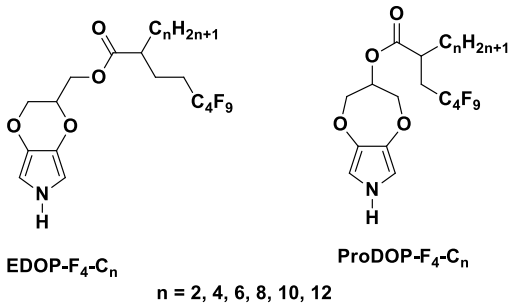

Scheme 1. Original monomers studied in this manuscript.

2. Experimental section

2.1. Monomer synthesis

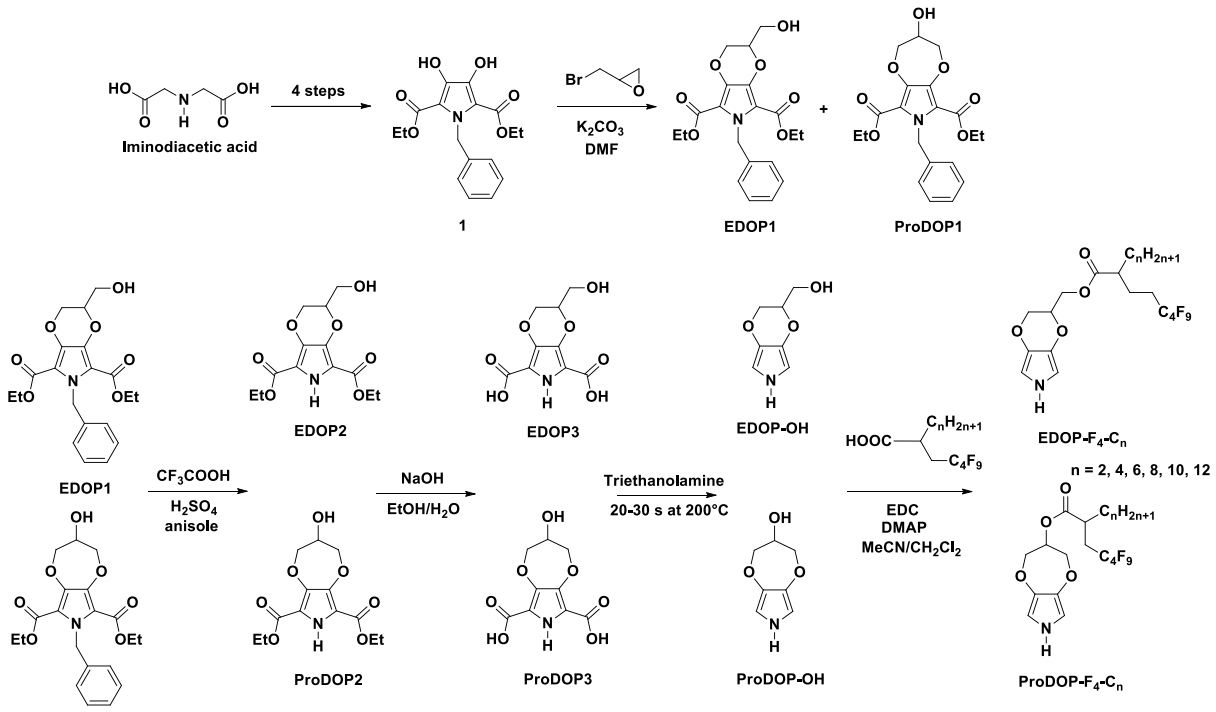

Scheme 2. Synthesis way to the monomers. (n = 2 to 12)

The monomers were synthesized according to publications reported in the literature. On the one hand, the key intermediates are the molecules coded ProDOP-OH and EDOP-OH obtained in eight steps from iminodiacetic acid (Scheme 2), thanks for example to a reaction with epibromohydrin [32]. On the other hand, acids with both alkyl (C_nH_{2n+1} with n = 2, 4, 6, 8, 10 and 12) and fluorinated (C_4F_9) chains were synthesized in four steps from diethyl malonate: two nucleophilic substitution, saponification/acidification and decarboxylation (Scheme 3) [36].

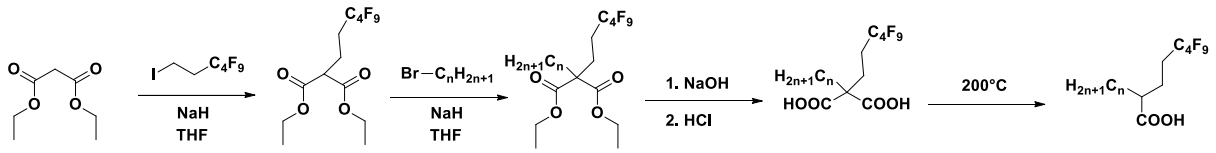

Scheme 3. Synthesis way of the mixed (hydrocarbon and fluorocarbon) acids (n = 2 to 12).

Then, the acids were grafted by simple esterification reaction. For that, 1.2 equiv. of the corresponding acid, 0.31 g of *N*-(3-dimethylaminopropyl)-*N*-ethylcarbodiimide hydrochloride (EDC) (0.0015 mol, 1.2 equiv.) and 20 mg of *N*,*N*-dimethylaminopyridine (DMAP) were added to 20 mL of absolute dichloromethane. After stirring for 30 min, the mixture was added to 20 mL of absolute acetonitrile containing 0.2 g of ProDOP-OH or EDOP-OH (0.0013 mol, 1 equiv.). After 1 day, the products were purified by column chromatography using

tetrahydrofuran/petroleum ether 60:40 as eluent. 10% of triethylamine was added in the silica gel and in the eluent because of the product sensitivity.

(3,6-dihydro-2*H*-[1,4]dioxino[2,3-*c*]pyrrol-2-yl)methyl 2-ethyl-5,5,6,6,7,7,8,8,8-nonafluorooctanoate (EDOP-F_4-C_2). Yield 53%; beige Crystalline solid; δ_H(200 MHz, $CDCl_3$): 7.15 (s, 1H), 6.19 (m, 2H), 4.37 (m, 3H), 4.20 (m, 1H), 4.04 (m, 1H), 2.45 (m, 1H), 2.00 (m, 4H), 1.66 (m, 2H), 0.94 (t, J = 7.4 Hz, 3H); δ_C(200 MHz, $CDCl_3$): 174.56, 132.08, 131.77, 98.67, 98.47, 72.06, 66.45, 62.65, 45.95, 34.22, 30.30, 25.25, 11.44; MS (ESI LC/MS): $[MH]^+$ = 472.07.

(3,6-dihydro-2*H*-[1,4]dioxino[2,3-*c*]pyrrol-2-yl)methyl 2-butyl-5,5,6,6,7,7,8,8,8-nonafluorooctanoate (EDOP-F_4-C_4). Yield 77%; beige Crystalline solid; δ_H(200 MHz, $CDCl_3$): 7.11 (s, 1H), 6.19 (m, 2H), 4.35 (m, 3H), 4.21 (m, 1H), 4.03 (m, 1H), 2.48 (m, 1H), 1.90 (m, 4H), 1.60 (m, 2H), 1.29 (m, 4H), 0.89 (t, J = 6.6 Hz, 3H); δ_C(200 MHz, $CDCl_3$): 174.74, 132.09, 131.81, 98.67, 98.47, 72.05, 66.45, 62.65, 44.51, 31.91, 30.30, 29.20, 28.61, 22.48, 13.83; MS (ESI LC/MS): $[MH]^+$ = 500.07.

(3,6-dihydro-2*H*-[1,4]dioxino[2,3-*c*]pyrrol-2-yl)methyl 5,5,6,6,7,7,8,8,8-nonafluoro-2-hexyloctanoate (EDOP-F_4-C_6). Yield 71%; beige Crystalline solid; δ_H(200 MHz, $CDCl_3$): 7.09 (s, 1H), 6.19 (m, 2H), 4.35 (m, 3H), 4.20 (m, 1H), 4.03 (m, 1H), 2.46 (m, 1H), 2.08 (m, 4H), 1.64 (m, 2H), 1.26 (m, 8H), 0.87 (t, J = 6.0 Hz, 3H); δ_C(200 MHz, $CDCl_3$): 174.74, 132.10, 131.80, 98.67, 98.47, 72.00, 66.46, 62.65, 44.52, 32.17, 31.80, 29.69, 29.41, 29.33, 29.19, 28.60, 27.07, 22.62, 14.06; MS (ESI LC/MS): $[MH]^+$ = 528.13.

(3,6-dihydro-2*H*-[1,4]dioxino[2,3-*c*]pyrrol-2-yl)methyl 2-(3,3,4,4,5,5,6,6,6-nonafluorohexyl)decanoate (EDOP-F_4-C_8). Yield 56%; beige Crystalline solid; δ_H(200 MHz, $CDCl_3$): 7.16 (s, 1H), 6.19 (m, 2H), 4.36 (m, 3H), 4.20 (m, 1H), 4.02 (m, 1H), 2.47 (m, 1H), 2.10 (m, 4H), 1.66 (m, 2H), 1.25 (m, 12H), 0.87 (t, J = 6.0 Hz, 3H); δ_C(200 MHz, $CDCl_3$): 174.74, 132.08, 131.77, 98.65, 98.46, 72.04, 66.47, 62.64, 44.52, 35.52, 34.21, 32.18, 31.81, 30.30, 29.40, 29.34, 29.18, 27.03, 22.66, 14.07; MS (ESI LC/MS): $[MH]^+$ = 556.13.

(3,6-dihydro-2*H*-[1,4]dioxino[2,3-*c*]pyrrol-2-yl)methyl 2-(3,3,4,4,5,5,6,6,6-nonafluorohexyl)dodecanoate (EDOP-F_4-C_{10}). Yield 72%; beige Crystalline solid; δ_H(200 MHz, $CDCl_3$): 7.15 (s, 1H), 6.19 (m, 2H), 4.35 (m, 3H), 4.20 (m, 1H), 4.05 (m, 1H), 2.50 (m, 1H), 2.00 (m, 4H), 1.70 (m, 2H), 125 (m, 16H), 0.87 (t, J = 6.3 Hz, 3H); δ_C(200 MHz, $CDCl_3$): 174.74, 132.09, 131.77, 98.65, 98.46, 72.02, 66.48, 62.65; 44.52, 35.53, 34.21,

32.18, 31.88, 30.30, 29.65, 29.57, 29.47, 29.42, 29.39, 29.30, 27.20, 22.61, 14.08; MS (ESI LC/MS): $[MH]^+$ = 584.13.

(3,6-dihydro-2H-[1,4]dioxino[2,3-c]pyrrol-2-yl)methyl 2-(3,3,4,4,5,5,6,6,6-nonafluorohexyl)tetradecanoate (EDOP-F_4-C_{12}). Yield 86%; beige Crystalline solid; δ_H(200 MHz, $CDCl_3$): 7.10 (s, 1H), 6.19 (m, 2H), 4.35 (m, 3H), 4.21 (m, 1H), 4.02 (m, 1H), 2.50 (m, 1H), 2.00 (m, 4H), 1.70 (m, 2H), 1.25 (m, 20H), 0.94 (t, *J* = 6.3 Hz, 3H); δ_C(200 MHz, $CDCl_3$): 174.74, 132.10, 131.79, 98.66, 98.47, 72.05, 66.46, 62.64, 44.53, 35.52, 34.21, 32.21, 31.90, 30.30, 29.63, 29.55, 29.42, 29.39, 29.34, 27.08, 22.68, 14.10; MS (ESI LC/MS): $[MH]^+$ = 612.20.

2,3,4,7-tetrahydro-[1,4]dioxepino[2,3-*c*]pyrrol-3-yl 2-ethyl-5,5,6,6,7,7,8,8,8-nonafluorooctanoate (ProDOP-F_4-C_2). Yield 53%; beige Crystalline solid; δ_H(200 MHz, $CDCl_3$): 7.19 (s, 1H), 6.31 (d, *J* = 3.2 Hz, 2H), 5.20 (m, 1H), 4.22 (dd, *J* = 12.6 Hz, *J* = 4.8 Hz, 2H), 4.05 (dd, *J* = 12.6 Hz, *J* = 2.4 Hz, 2H), 2.49 (m, 1H), 2.00 (m, 2H), 1.69 (m, 4H), 0.96 (t, *J* = 7.4 Hz, 3H); δ_C(200 MHz, $CDCl_3$): 174.28, 138.85, 103.17, 73.04, 72.46, 45.94, 34.22, 30.31, 25.28, 11.41; MS (ESI LC/MS): $[MH]^+$ = 472.00.

2,3,4,7-tetrahydro-[1,4]dioxepino[2,3-c]pyrrol-3-yl 2-butyl-5,5,6,6,7,7,8,8,8-nonafluorooctanoate (ProDOP-F_4-C_4). Yield 62%; beige Crystalline solid; δ_H(200 MHz, $CDCl_3$): 7.30 (s, 1H), 6.30 (d, *J* = 3.3 Hz, 2H), 5.19 (m, 1H), 4.22 (dd, *J* = 12.5 Hz, *J* = 4.8 Hz, 2H), 4.05 (dd, *J* = 12.5 Hz, *J* = 2.6 Hz, 2H), 2.49 (m, 1H), 2.07 (m, 4H), 1.74 (m, 2H), 1.30 (m, 4H), 0.89 (t, *J* = 6.7 Hz, 3H); δ_C(200 MHz, $CDCl_3$): 174.45, 138.82, 103.13, 73.01, 72.43, 44.49, 31.86, 30.30, 29.17, 26.90, 22.48, 13.83; MS (ESI LC/MS): $[MH]^+$ = 500.07.

2,3,4,7-tetrahydro-[1,4]dioxepino[2,3-c]pyrrol-3-yl 5,5,6,6,7,7,8,8,8-nonafluoro-2-hexyloctanoate (ProDOP-F_4-C_6). Yield 70%; beige Crystalline solid; δ_H(200 MHz, $CDCl_3$): 7.22 (s, 1H), 6.31 (d, *J* = 3.3 Hz, 2H), 5.19 (m, 1H), 4.22 (dd, *J* = 12.6 Hz, *J* = 4.9 Hz, 2H), 4.05 (dd, *J* = 12.6 Hz, *J* = 2.6 Hz, 2H), 2.53 (m, 1H), 2.02 (m, 4H), 1.80 (m, 2H), 1.26 (m, 8H), 0.87 (t, *J* = 6.3 Hz, 3H); δ_C(200 MHz, $CDCl_3$): 174.45, 138.84, 103.14, 73.01, 72.43, 44.52, 34.22, 32.19, 31.57, 30.31, 29.07, 26.99, 22.53, 14.01; MS (ESI LC/MS): $[MH]^+$ = 528.07.

2,3,4,7-tetrahydro-[1,4]dioxepino[2,3-c]pyrrol-3-yl 5,5,6,6,7,7,8,8,8-nonafluoro-2-hexyloctanoate (ProDOP-F_4-C_8). Yield 70%; dark beige Crystalline solid; δ_H(200 MHz, $CDCl_3$): 7.26 (s, 1H), 6.31 (d, *J* = 3.3 Hz, 2H), 5.19 (m, 1H), 4.22 (dd, *J* = 12.6 Hz, *J* =4.8 Hz, 2H), 4.05 (dd, *J* = 12.6 Hz, *J* = 2.4 Hz, 2H), 2.56 (m, 1H), 2.08 (m, 4H), 1.74 (m, 2H), 1.25 (m, 12H), 0.87 (t, *J* = 6.3 Hz, 3H); δ_C(200 MHz, $CDCl_3$): 174.45, 138.84, 103.13, 73.00,

72.43, 44.52, 35.52, 34.21, 32.18, 31.81, 30.30, 29.40, 29.34, 29.18, 27.03, 22.66, 14.07; MS (ESI LC/MS): $[MH]^+ = 556.07$.

2,3,4,7-tetrahydro-[1,4]dioxepino[2,3-c]pyrrol-3-yl 5,5,6,6,7,7,8,8,8-nonafluoro-2-hexyloctanoate (ProDOP-F_4-C_{10}). Yield 70%; dark beige Crystalline solid; δ_H(200 MHz, $CDCl_3$): 7.22 (s, 1H), 6.30 (d, J = 3.3 Hz, 2H), 5.20 (m, 1H), 4.22 (dd, J = 12.6 Hz, J = 4.9 Hz, 2H), 4.05 (dd, J = 12.6 Hz, J = 2.6 Hz, 2H), 2.55 (m, 1H), 2.12 (m, 4H), 1.78 (m, 2H), 1.25 (m, 16H), 0.88 (t, J = 6.4 Hz, 3H); δ_C(200 MHz, $CDCl_3$): 174.45, 138.84, 103.13, 73.00, 72.43, 44.52, 35.53, 34.21, 32.18, 31.89, 30.30, 29.56, 29.52, 29.39, 29.30, 27.04, 22.66, 14.08; MS (ESI LC/MS): $[MH]^+ = 584.20$.

2,3,4,7-tetrahydro-[1,4]dioxepino[2,3-c]pyrrol-3-yl 5,5,6,6,7,7,8,8,8-nonafluoro-2-hexyloctanoate (ProDOP-F_4-C_{12}). Yield 76%; dark beige Crystalline solid; δ_H(200 MHz, $CDCl_3$): 7.26 (s, 1H), 6.31 (d, J = 3.2 Hz, 2H), 5.19 (m, 1H), 4.22 (dd, J = 12.6 Hz, J = 4.9 Hz, 2H), 4.05 (dd, J = 12.6 Hz, J = 2.6 Hz, 2H), 2.53 (m, 1H), 2.07 (m, 4H), 1.77 (m, 2H), 1.25 (m, 20H), 0.88 (t, J = 6.4 Hz, 3H); δ_C(200 MHz, $CDCl_3$): 174.46, 138.84, 103.13, 73.00, 72.43, 44.52, 35.52, 34.21, 32.18, 31.90, 30.30, 29.62, 29.53, 29.39, 29.34, 26.90, 22.67, 14.09; MS (ESI LC/MS): $[MH]^+ = 612.07$.

2.2 Electrochemical parameters

The depositions were performed with an Autolab potentiostat from Metrohm. The electrolyte consisted in acetonitrile with 0.1 M of tetrabutylammonium perchlorate (Bu_4NClO_4). 10 mL of electrolyte and 0.01 M of monomer were inserted inside a glass cell. The connection to the potentiostat was performed with three electrodes. A saturated calomel electrode (SCE) was used as a reference electrode and a carbon rod was used as a counter-electrode. As a working electrode, a platinum tip was first used to electrochemically characterize the polymerization, while 2 cm^2 gold-coated silicon wafers were used for the surface characterization. After each deposition, the surfaces were washed acetonitrile and slowly dried.

2.3 Surface characterization

The surfaces were characterized to determine the surface morphology by scanning electron microscopy (SEM), the surface roughness by optical profilometry and the surface wettability by goniometry. For the SEM images, a 6700F microscope from JEOL was used after metallization. For the optical profilometry, a WYKO NT1100 optical profiling system from

Bruker was used to determine the arithmetic (*Ra*) and quadratic (*Rq*) surface roughness with the working mode High Mag Phase Shift Interference (PSI), the objective 50X, and the field of view 0.5X. Each data given is a mean of five measurements. For the goniometry, a DSA30 goniometer from Krüss was used. First, 2 μL water droplets were placed on the surface to determine the apparent contact angles at the triple point using the software Drop Shape Analysis. For the dynamic contact angles, the tilted-drop method was used using 6 μL water droplets placed on the surface and the surface was inclined until the droplet moves. The advanced and receding contact angle and as a consequence the hysteresis (H) were taken just before the droplet moving. When the droplet moves for a surface inclination (α) below 10°, the surface is superhydrophobic. When the droplet does not move whatever the surface inclination, the surface is called sticky or parahydrophobic.

3. Result and Discussion

The electrodepositions were performed in an electrolyte containing anhydrous acetonitrile and 0.1 M tetrabutylammonium perchlorate (Bu_4NClO_4). First, the monomer oxidation potentials were determined by cyclic voltammetry and were found to be around 1.05 and 1.15 V *vs* SCE. Then, cyclic voltammograms were realized in order to have information of the polymer growth on the working electrode (Fig.1 and Fig.2). The cyclic voltammograms are displayed in Figure and Figure. Unfortunately, due to the presence of both a hydrocarbon and a fluorocarbon chain, the growth of the polymer is highly affected by steric hindrance. Only with EDOP-F_4-C_8 the steric hindrance is minimized and the polymer could polymerize very easily by cyclic voltammetry. Indeed, it is extremely known that the presence of a substituent and especially its size and its rigidity can highly affect the polymerization because it changes the intra and intermolecular interactions. Moreover, there is steric hindrance whatever the polymerization method.

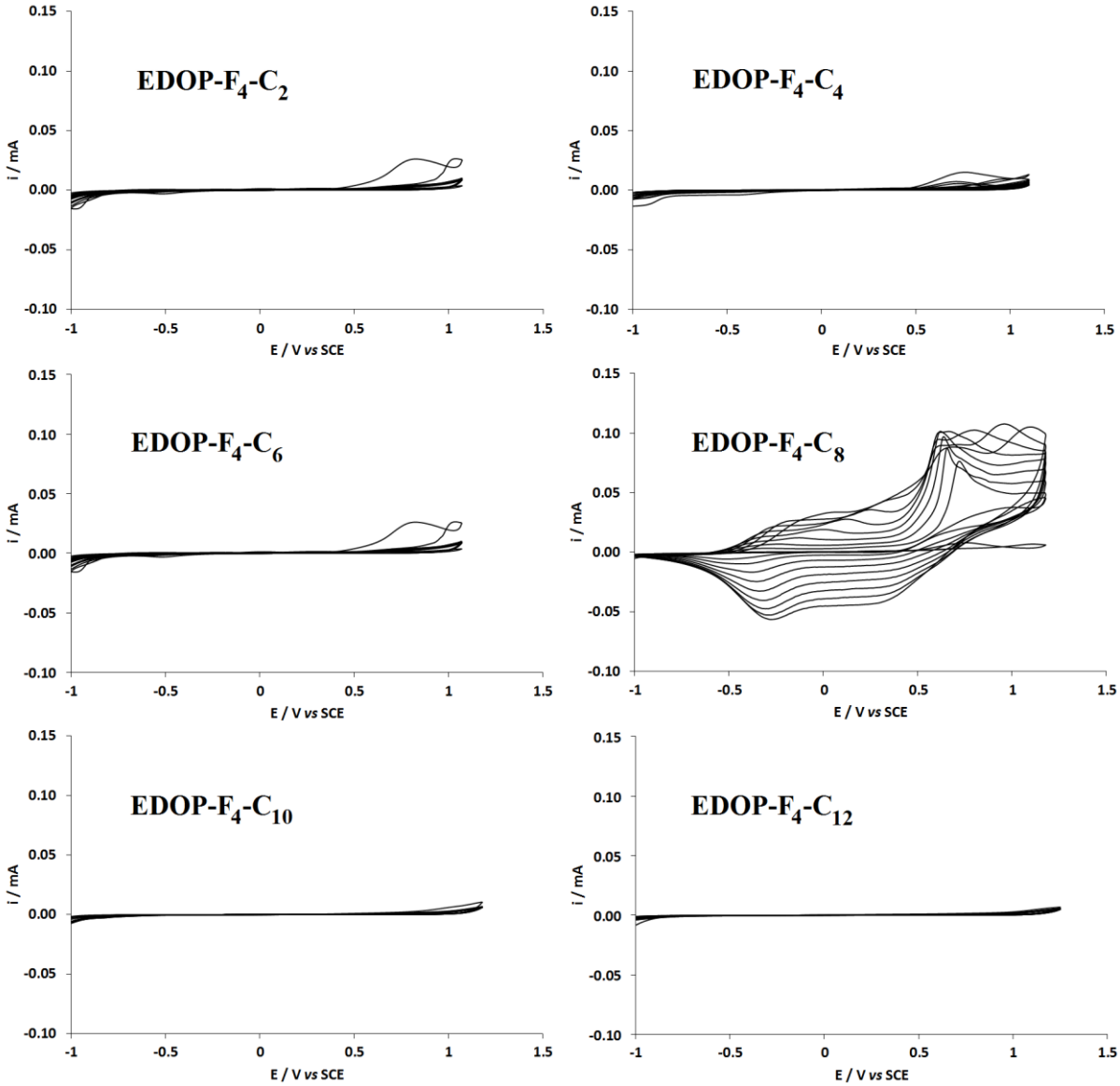

Figure 1. Cyclic voltammograms of the EDOP derivatives (0.01 M) in anhydrous acetonitrile with Bu_4NClO_4 (0.1 M); scan rate: 20 mV s^{-1}.

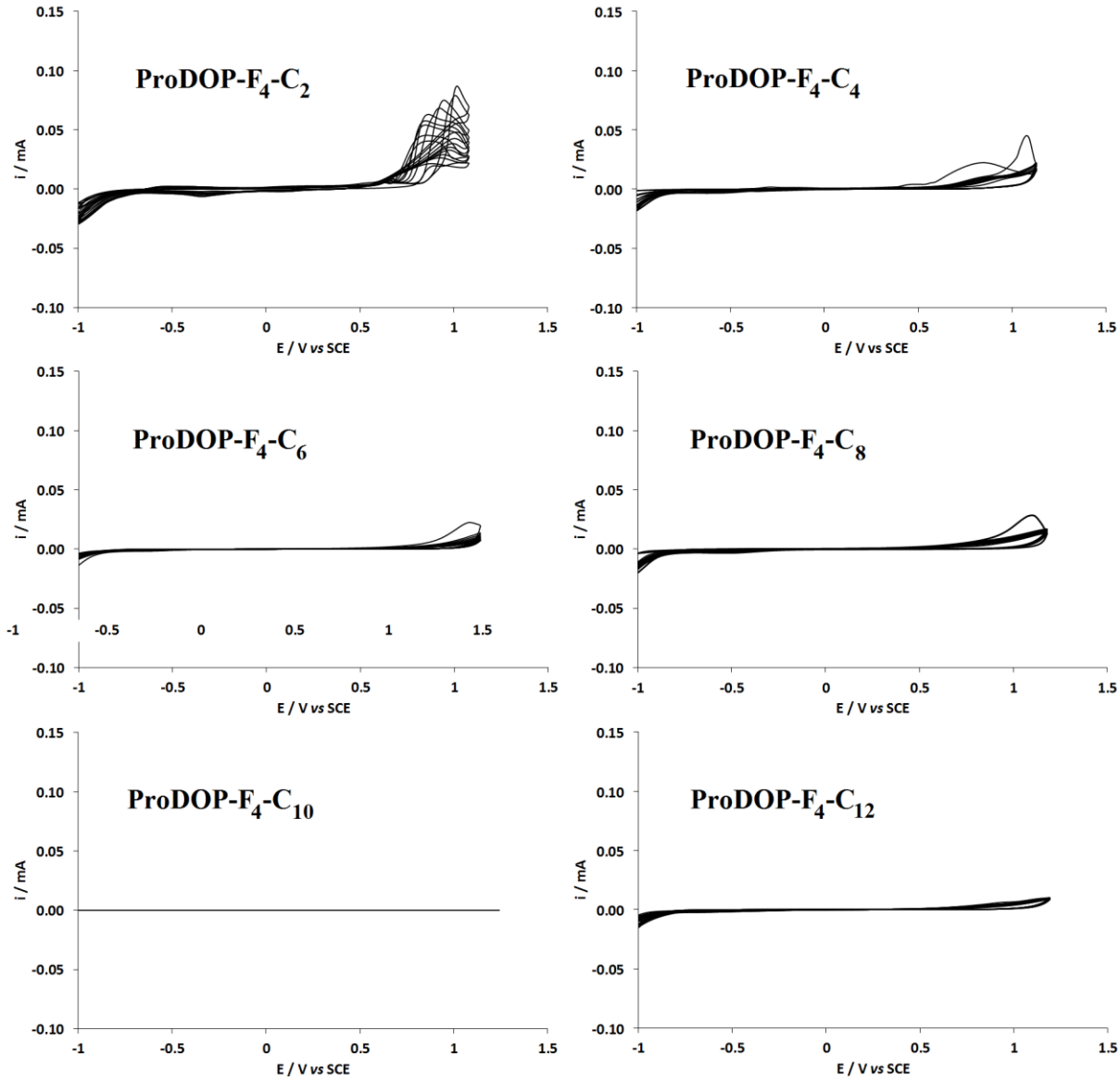

Figure 2. Cyclic voltammograms of the ProDOP derivatives (0.01 M) in anhydrous acetonitrile with Bu_4NClO_4 (0.1 M); scan rate: 20 mV s^{-1}.

Hence, for the surface characterization, using these monomers it was preferable to deposit the polymers at constant potential rather than by cyclic voltammetry. The deposition at constant is an extremely interesting deposition technique because the amount of polymer can be easily controlled with the deposition charge (Qs). For all the monomers, we have chosen to vary Qs from 12.5 to 400 mC cm^2. With this technique, it was possible to obtain polymer films with all the EDOP derivatives and the ProDOP derivatives with long alkyl chains ($\geq C_8$). The ProDOP polymers with shorter alkyl chains were found to be too soluble. With longer alkyl chains, even if the polymer conductivity is affected, the polymers could be easily deposited because of their high insolubility. This is possible thanks to the exceptional polymerization capacity of EDOP and ProDOP monomers [26-28]. The presence of the two oxygen atoms on

the 3- and 4-position highly reduces the monomer and polymer oxidation potential while their presence also suppresses polymerization defects.

First, the polymer films were characterized by infrared (IR) spectroscopy. For that, it was preferable to reduce the polymers because the dopants absorb in IR. The reduction was performed at constant potential of -1 V *vs* SCE for 15 mn. Examples of IR are given in Figure 3. As expected, the spectra of PEDOP and PProDOP are close because the chemical functions are the same. For example, the spectra display bands at 3400 cm^{-1} for the stretching of N–H bonds, at 2930 and 2855 cm^{-1} for the stretching of C–H bonds, at 1735 cm^{-1} for the stretching of C=O bonds and at 1080 cm^{-1} for the stretching of C–F bonds.

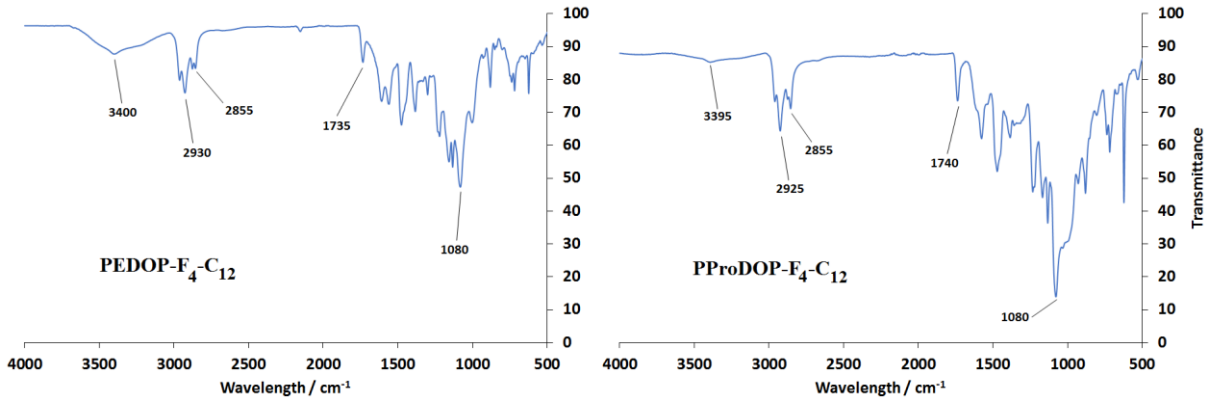

Figure 3. Infrared spectra of PEDOP-F_4-C_{12} and PProDOP-F_4-C_{12}.

Then, the surface morphology was investigated by SEM. Using these monomers, it was observed both the presence of both nanoparticles and wrinkles. With the EDOP derivatives (Figure 4 and Figure 5), the presence of ultra-small nanoparticles is observed with the shortest alkyl chains (C_2 and C_4) but the nanoparticles do not cover all the surface. As the alkyl chain length increases, the size of the nanoparticles increases, and they cover almost all the surface using intermediate sizes (C_6 and C_8). Using these chains, the surfaces are extremely rough and porous. Using longest alkyl chains (C_{10} and C_{12}), the size of the nanoparticles increases but their number is highly reduced. For the wrinkles, they seem to increase in size with the alkyl chain length until to be extremely large for the longest alkyl chains (C_{12}).

Concerning the surface wettability, the presence of both nanoparticles and wrinkles induce a high increase in surface hydrophobicity, as shown in Table 1. Here, the standard deviation of the data can be relatively important because the wrinkles are not homogeneously distributed on the surface. The highest surface properties with θ_w up to 141° were obtained with EDOP-

F_4-C_6 and EDOP-F_4-C_8 for Qs = 400 mC cm^2 because of the high coverage in nanoparticles leading surfaces with high roughness and porosity.

Moreover, dynamic contact angles shown that these surfaces are also extremely sticky (parahydrophobic), as observed on rose petals (Figure 6) [11-14]. Indeed, water droplets remain completely stuck on these surfaces whatever the surface inclination. These parahydrophobic properties are extremely interesting and this kind of surfaces could be used in the future in water harvesting systems. As reported in the literature, parahydrophobic properties are intermediate state between the Wenzel and the Cassie-Baxter states [11-13]. These states can be explained with the Cassie-Baxter equation [37] because there is air between the surface and the water droplet, even if the amount of air should not be too important otherwise superhydrophobic properties can be obtained. Moreover, it is normal that there is no direct relationship between θ_w and the surface roughness or even the roughness parameter (r) of the Wenzel equation [38] because the Cassie-Baxter equation is not related to them.

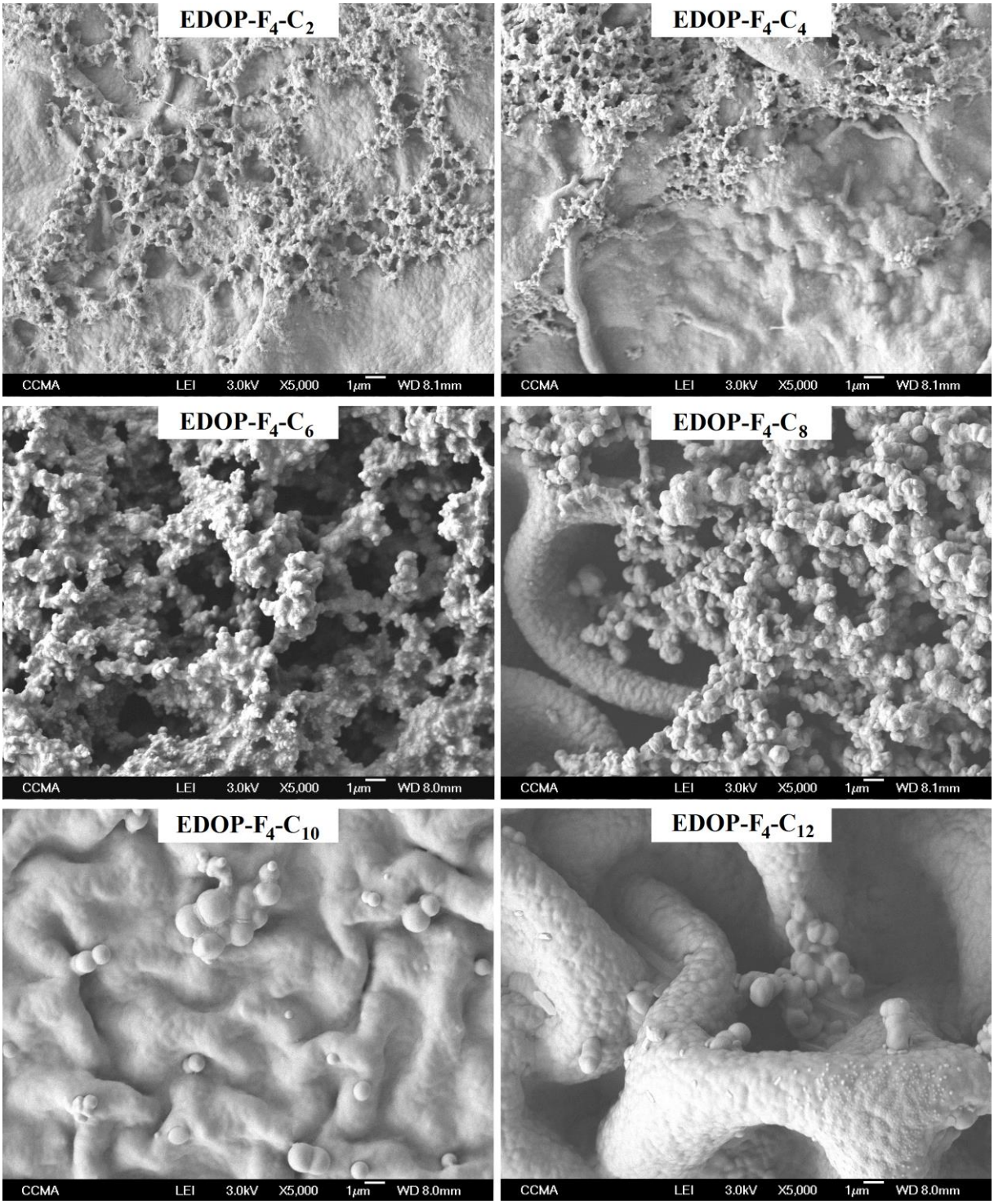

Figure 4. SEM images of the polymer films obtained with the EDOP derivatives with a deposition charge of 400 mC cm^{-2}; Magnification: 5000x.

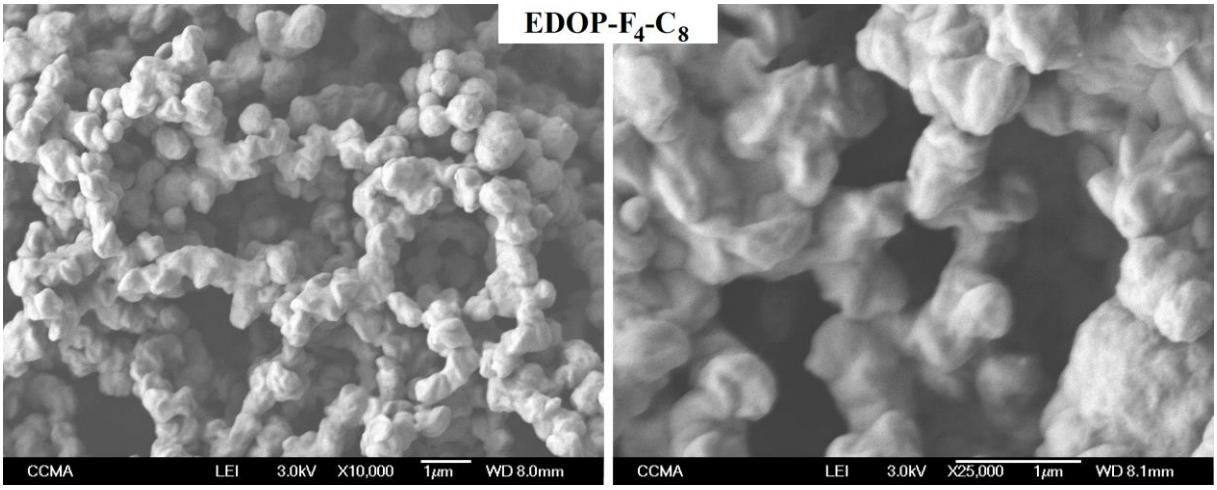

Figure 5. SEM images of the polymer films obtained with the EDOP-F_4-C_8 derivatives with a deposition charge of 400 mC cm^{-2}; Magnification: 10000x and 25000x.

Table 1. Roughness (Ra and Rq) and wettability data for the PEDOP polymers.

Polymer	Deposition charge [mC cm^{-2}]	Ra [nm]	Rq [nm]	θ_w [deg]
PEDOP-F_4-C_2	12.5	33 ± 10	53 ± 17	95.7 ± 3.7
	25	85 ± 10	133 ± 14	106.2 ±1.4
	50	217 ± 34	297 ± 45	112.5 ± 2.2
	100	558 ± 31	734 ± 30	98.1 ± 3.6
	200	611 ± 58	793 ± 84	112.1 ± 6.8
	400	622 ± 40	832 ± 66	119.6 ± 5.6
PEDOP-F_4-C_4	12.5	34 ± 12	48 ± 3	107.0 ± 0.7
	25	169 ± 14	236 ± 20	110.5 ± 3.1
	50	307 ± 20	419 ± 26	109.8 ± 4.6
	100	571 ± 35	725 ± 40	107.6 ± 7.5
	200	565 ± 30	722 ± 34	106.6 ± 9.8
	400	695 ± 31	943 ±74	115.3 ± 9.1
PEDOP-F_4-C_6	12.5	33 ± 4	42 ± 6	104.8 ± 2.1
	25	67 ± 4	98 ± 16	112.4 ± 2.6
	50	98 ± 18	146 ± 29	114.8 ± 1.8
	100	264 ± 19	335 ± 58	120.0 ± 6.2
	200	500 ± 43	645 ± 52	135.4 ± 5.2
	400	623 ± 24	854 ± 56	141.0 ± 2.4
PEDOP-F_4-C_8	12.5	39 ± 6	55 ± 17	107.2 ± 0.8
	25	58 ± 5	78 ± 10	118.6 ± 5.0
	50	164 ± 21	214 ± 27	119.8 ± 6.4
	100	170 ± 45	245 ± 62	129.8 ± 8.1
	200	352 ± 76	460 ± 97	126.7 ± 7.1

	400	402 ± 92	524 ± 108	140.7 ± 5.1
PEDOP-F_4-C_{10}	12.5	54 ± 15	85 ± 48	104.7 ± 0.8
	25	100 ± 30	147 ± 60	105.5 ± 0.6
	50	44 ± 12	56 ± 13	105.4 ± 1.9
	100	62 ± 20	93 ± 46	103.5 ± 0.6
	200	103 ± 76	154 ± 36	101.0 ± 0.6
	400	372 ± 120	504 ± 175	104.1 ± 3.8
PEDOP-F_4-C_{12}	12.5	20 ± 7	25 ± 10	106.2 ± 1.9
	25	28 ± 3	35 ± 3	106.7 ± 1.3
	50	36 ± 7	42 ± 7	107.1 ± 0.5
	100	210 ± 50	270 ± 55	119.8 ± 7.2
	200	522 ± 70	677 ± 85	118.7 ± 10.2
	400	392 ± 110	550 ± 120	133.2 ± 1.7

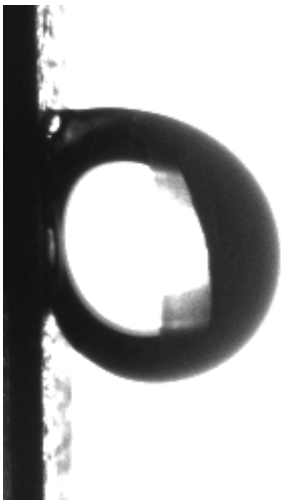

Figure 6. Picture of a water droplet on a surface inclined to 90° obtained with EDOP-F_4-C_8 and with a deposition charge of 400 mC cm^{-2}.

Using the ProDOP derivatives, unfortunately it was possible to obtain polymer films but only using long alkyl chains (Figure 7). Here, it was observed also the presence of wrinkles and nanoparticles. The surface properties were in general lower (Table 2). Using ProDOP-F_4-C_{12}, it was possible to reach θ_w = 133.2° due to the formation of very large wrinkles.

Hence, the presence of wrinkles seems to be extremely interesting to reach parahydrophobic properties. Indeed, it is known in the literature, that the surface hydrophobicity and water adhesion of wrinkled surfaces can be controlled with the wrinkles geometrical parameters such as the wrinkle wavelength [39-41]. For applications in water harvesting, for example, it is preferable to have the highest θ_w while having strong water adhesion. Here, is was possible either by covering with nanoparticles and/or by increasing the alkyl chain length.

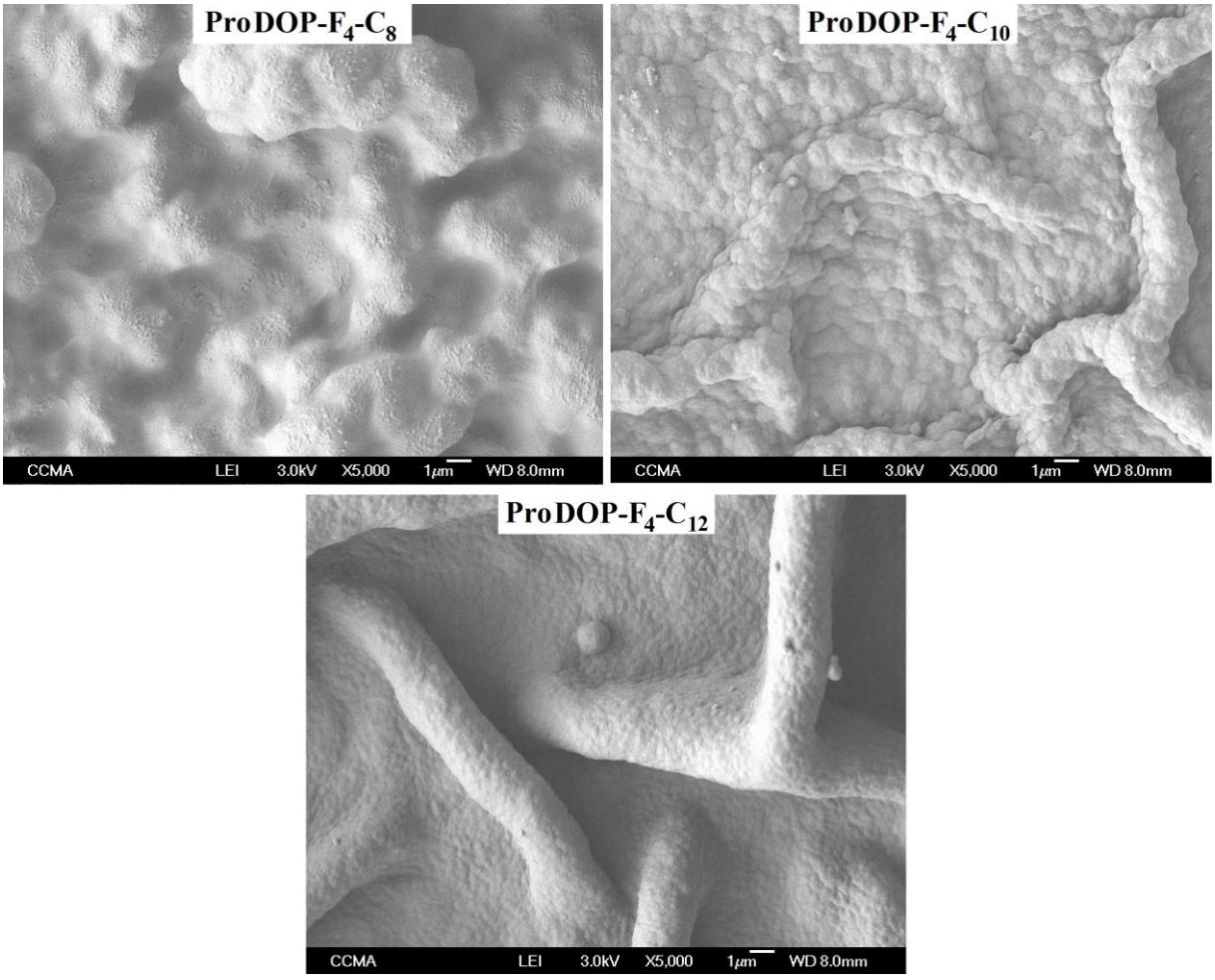

Figure 7. SEM images of the polymer films obtained with the ProDOP derivatives with a deposition charge of 400 mC cm^{-2}; Magnification: 5000x.

Table 2. Roughness (Ra and Rq) and wettability data for the ProDOP polymers.

Polymer	Deposition charge [mC cm^{-2}]	Ra [nm]	Rq [nm]	θ_w [deg]
ProDOP-F_4-C_8	12.5	41 ± 11	52 ± 16	106.4 ± 0.8
	25	45 ± 9	62 ± 14	109.4 ± 1.6
	50	131 ± 21	212 ± 10	105.4 ± 4.8
	100	217 ± 70	291 ± 102	108.6 ± 4.1
	200	265 ± 41	354 ± 53	111.7 ± 4.4
	400	459 ± 113	610 ± 140	119.8 ± 6.1
ProDOP-F_4-C_{10}	12.5	28 ± 9	39 ± 13	106.9 ± 1.9
	25	18 ± 3	30 ± 19	107.7 ± 0.9
	50	75 ± 17	96 ± 24	112.6 ± 2.7
	100	370 ± 127	544 ± 165	118.8 ± 7.2
	200	404 ± 31	532 ± 37	116.8 ± 1.9
	400	623 ± 69	822 ± 95	114.5 ± 10.0
ProDOP-F_4-C_{12}	12.5	37 ± 6	72 ± 25	104.7 ± 0.9
	25	45 ± 10	64 ± 12	104.6 ± 3.4
	50	70 ± 7	108 ± 12	107.4 ± 3.8
	100	272 ± 27	353 ± 37	126.8 ± 2.8
	200	504 ± 44	661 ± 64	134.7 ± 3.1
	400	407 ± 52	526 ± 55	128.9 ± 3.6

4. Conclusion

We reported the electrodeposition of PEDOP and ProDOP with both a short fluorocarbon chain (C_4F_9) and an alkyl chain of various length (C_2H_5 to $C_{12}H_{25}$). The surface properties could be controlled with the polymerizable core (EDOP or ProDOP) and the alkyl chain length. The PEDOP polymers could be easier electrodeposited because there were more insoluble while the ProDOP could be also electrodeposited but only with long alkyl chains ($\geq$ C_8H_{17}). With these derivatives, both the nanoparticles and wrinkles were observed. Parahydrophobic properties (θ_w) $\approx$ 141° and extremely strong water adhesion) were obtained with EDOP monomers and intermediate alkyl chains (C_6H_{13} and C_8H_{17}). These surface properties are extremely interesting and could be applied in the future for water harvesting systems, for example.

References

[1] K. Liu, X. Yao, L. Jiang, Recent developments in bio-inspired special wettability, Chem. Soc. Rev. 39 (2013) 3240–3255.

[2] H. Liu, Y. Wang, J. Huang, Z. Chen, G. Chen, Y. Lai, Bioinspired surfaces with superamphiphobic properties: concepts, synthesis, and applications, Adv. Funct. Mater. 28 (2018) 1707415.

[3] M. Nosonovsky, B. Bhushan, Superhydrophobic surfaces and emerging applications: non-adhesion, energy, green engineering, Curr. Opin. Colloid Interface Sci. 14 (2009) 270–280.

[4] X. Tian, T. Verho, R. H. A. Ras, Moving superhydrophobic surfaces toward real-world applications, Science 352 (2016) 142–143.

[5] T. Darmanin, F. Guittard, Superhydrophobic and superoleophobic properties in nature, Mater. Today18 (2015) 273–285.

[6] Z. Sun, T. Liao, K. Liu, L. Jiang, J. H. Kim, S. X. Dou, Fly-eye inspired superhydrophobic anti-fogging inorganic nanostructures, Small 10 (2014) 3001–3006.

[7] Y. Dou, D. Tian, Z. Sun, Q. Liu, N. Zhang, J. H. Kim, Lei Jiang, S. X. Dou, Fish gill inspired crossflow for efficient and continuous collection of spilled oil, ACS Nano 11 (2017) 2477–2485.

[8] K. Koch, B. Bhushan, W. Barthlott, Multifunctional surface structures of plants: an inspiration for biomimetics, Prog. Mater. Sci. 54 (2009) 137–178.

[9] M. Sun, G.S. Watson, Y. Zheng, J. A. Watson, A. Liang, Wetting properties on nanostructured surfaces of cicada wings, J. Exp. Biol. 212 (2009) 3148–3155.

[10] Z. Sun, T. Liao, L. Sheng, J.H. Kim, S.X. Dou, J. Bell, Fly compound-eye inspired inorganic nanostructures with extraordinary visible-light responses, Mater. Today Chem. 1–2 (2016) 84–89.

[11] L. Feng, Y. Zhang, J. Xi, Y. Zhu, N. Wang, F. Xia, L. Jiang, Petal effect: a superhydrophobic state with high adhesive force, Langmuir 24 (2008) 4114–4119.

[12] B. Bhushan, M. Nosonovsky, M The rose petal effect and the modes of superhydrophobicity, Phil. Trans. R. Soc. A 368 (2010) 4713–4728.
[13] A. Marmur, Hydro- hygro- oleo- omni-phobic? terminology of wettability classification. Soft Matter 8 (2012) 6867–6870.

[14] C. R. Szczepanski, T. Darmanin, F. Guittard, Recent advances in the study and design of parahydrophobic surfaces: From natural examples to synthetic approaches, Adv. Colloid Interface Sci.241 (2017) 37–61.

[15] J. Yong, F. Chen, M. Li, Q. Yang, Y. Fang, J. Huo, X. Hou, Remarkably simple achievement of superhydrophobicity, superhydrophilicity, underwater superoleophobicity, underwater superoleophilicity, underwater superaerophobicity, and underwater superaerophilicity on femtosecond laser ablated PDMS surfaces, J. Mater. Chem. A 5 (2017) 25249–25257.
[16] Y. Cheng, H. Yang, Y. Yang, J. Huang, K. Wu, Z. Chen, X. Wang, C. Lin, Y. Lai, Progress in TiO_2 nanotube coatings for biomedical applications: a review, J. Mater. Chem. B 6 (2018) 1862–1886.
[17] Z. Wang, M. Lehtinen, G. Liu, Universal Janus filters for the rapid separation of oil from emulsions stabilized by ionic or nonionic surfactants, Angew. Chem. Int. Ed. 56 (2017) 12892–12897.
[18] A. Kharitonov, J. Zha, M. Dubois, Tunable hydrophylicity/hydrophobicity of fluorinated carbon nanotubes via graft polymerization of gaseous monomers, J. Fluorine Chem. 178 (2015) 279–285.
[19] Z. Sun, T. Liao, K. Liu, L. Jiang, J. H. Kim, S. X. Dou, Robust superhydrophobicity of hierarchical ZnO hollow microspheres fabricated by two-step self-assembly, Nano Res. 6 (2013) 726–735.
[20] T. Darmanin, G. Godeau, F. Guittard, Superhydrophobic, superoleophobic and underwater superoleophobic conducting polymer films, Surf. Innovations, DOI: 10.1680/jsuin.18.00006.
[21] S. Roquet, P. Leriche, I. Perepichka, B. Jousselme, E. Levillain, P. Frère, J. Roncali, 3,4-Phenylenedioxythiophene (PheDOT): a novel platform for the synthesis of planar substituted π–donor conjugated systems, J. Mater. Chem. 14 (2004) 1396–1400.
[22] M. P. Krompiec, S. N. Baxter, E. L. Klimareva, D. S. Yufit, D. G. Congrave, T. K. Britten, I. F. Perepichka, 3,4-Phenylenedioxythiophenes (PheDOTs) functionalized with

electron-withdrawing groups and their analogs for organic electronics, J. Mater. Chem. C 6 (2018) 3743–3756.
[23] H.-A. Lin, S.-C. Luo, B. Zhu, C. Chen, Y. Yamashita, H.-h. Yu, Molecular or nanoscale structures? The deciding factor of surface properties on functionalized poly(3,4-ethylenedioxythiophene) nanorod arrays, Adv. Funct. Mater. 23 (2013) 3212–3219.
[24] L. Qu, G. Shi, F. Chen, J. Zhang, Electrochemical growth of polypyrrole microcontainers, Macromolecules 36 (2003) 1063–1067.
[25] F.A. Arroyave, J.R. Reynolds, 3,4-Propylenedioxypyrrole-based conjugated oligomers via Pd-mediated decarboxylative cross coupling, Org. Lett. 12 (2010) 1328–1331.
[26] K. Zong, J.R. Reynolds, Poly(3,4-alkylenedioxypyrrole)s: highly stable electronically conducting and electrochromic polymers, Macromolecules 33 (2000) 7051–7061.
[27] R.M. Walczak, J.R. Reynolds, Poly(3,4-alkylenedioxypyrroles): the PXDOPs as versatile yet under utilized electroactive and conducting polymers, Adv. Mater. 18 (2006) 1121–1131.
[28] P. Schottland, K. Zong, C.L. Gaupp, B.-C. Thompson, C.A. Thomas, I. Giurgiu, R.Hickman, A. Khalil, K.A. Abboud, J.R. Reynolds, 3,4-Alkylenedioxypyrroles: functionalized derivatives as monomers for new electron-rich conducting and electroactive polymers, J. Org. Chem. 66 (2001) 6873–6882.
[29] C. Mortier, T. Darmanin, F. Guittard, 3,4-Ethylenedioxypyrrole (EDOP) monomers with aromatic substituents for parahydrophobic surfaces by electropolymerization, Macromolecules 48 (2015) 5188–5195
[30] D. Diouf, A. Diouf, C. Mortier, T. Darmanin, S.Y. Dieng, F. Guittard, Poly(3,4-propylenedioxypyrrole) nanofibers with branched alkyl chains by electropolymerization to obtain sticky surfaces with high contact angles, ChemistrySelect 2 (2017) 9490–9494.
[31] C. Mortier, T. Darmanin, F. Guittard, Major influence of the hydrophobic chain length in the formation of poly(3,4-propylenedioxypyrrole) (PProDOP) nanofibers with special wetting properties, Mater. Today Chem. 7(2018) 65–75.
[32] C. Mortier, T. Darmanin, F. Guittard, Direct electrodeposition of superhydrophobic and highly oleophobic poly(3,4-ethylenedioxypyrrole) (PEDOP) and poly(3,4-propylenedioxypyrrole) (PProDOP) nanofibers, ChemNanoMat 3 (2017) 885–894.
[33] C. E. Mueller, A. O. De Silva, J. Small, M. Williamson, X. Wang, A. Morris, S. Katz, M. Gamberg, D. C. G. Muir, Biomagnification of perfluorinated compounds in a remote terrestrial food chain: lichen–caribou–wolf, Environ. Sci. Technol. 45 (2011) 8665–8673.

[34] M. Houde, J. W. Martin, R. J. Letcher, K. R. Solomon, D. C. G. Muir, Biological monitoring of polyfluoroalkyl substances: a review, Environ. Sci. Technol. 40 (2006) 3463–3473.

[35] J. P. Giesy, K. Kannan, Global distribution of perfluorooctane sulfonate in wildlife, Environ. Sci. Technol. 35 (2001) 1339–1342.

[36] J. El-Maiss, T. Darmanin, E. Taffin de Givenchy, S. Amigoni, J. Eastoe, M. Sagisaka, F. Guittard, Superhydrophobic surfaces with low and high adhesion made from mixed (hydrocarbon and fluorocarbon) 3,4-propylenedioxythiophene monomers, J. Polym. Sci., Part B: Polym. Phys. 52 (2014) 782–788.

[37] A.B.D. Cassie, S. Baxter, Wettability of porous surfaces, Trans. Faraday Soc. 5 (1944) 546–551.

[38] R.N. Wenzel, Resistance of solid surfaces to wetting by water, Ind. Eng. Chem. 28 (1936) 988–994.

[39] E. P. Chan, E. J. Smith, R. C. Hayward, A. J. Crosby, Surface wrinkles for smart adhesion, Adv. Mater. 20 (2008) 711–716.

[40] Won-Kyu Lee, Woo-Bin Jung, Sidney R. Nagel, and Teri W. Odom, Stretchable superhydrophobicity from monolithic, three-dimensional hierarchical wrinkles, Nano Lett. 16 (2016) 3774–3779.

[41] J. El-Maiss, T. Darmanin, E. Taffin de Givenchy, F. Guittard, Elaboration of superhydrophobic surfaces containing nanofibers and wrinkles with controllable water and oil adhesion, Macromol. Mater. Eng. 299 (2014) 959–965.

Graphical Abstract

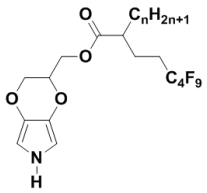

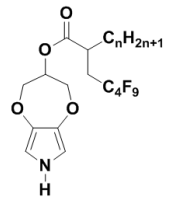

n = 2, 4, 6, 8, 10, 12